LULEÅ
UNIVERSITY
OF TECHNOLOGY

LICENTIATE THESIS

Multiphase Flow Measurements Using Ultrasound

JOHAN CARLSON

Department of Computer Science and Electrical Engineering
Division of Industrial Electronics

Multiphase Flow Measurements Using Ultrasound

Johan Carlson

Luleå University of Technology
Division of Industrial Electronics
Luleå, Sweden

December 1999

Supervisors:

Professor Jerker Delsing and Professor Anders Grennberg
Luleå University of Technology.

Abstract

In process industries such as for example the oil and gas industry, the paper pulp industry, and the mining industry, multiphase flows are common. It is often of interest to measure the mass fractions of the different the phases. In for example the mining industry, iron ore powder is transported using water, and there is a need of measurement techniques to monitor the particle mass fraction. Most existing techniques are either invasive, inaccurate, or too slow to be used in an on-line manner.

The long-term goal of this research project is to develop a method for measuring mass fractions and mass fraction velocities, using ultrasound. The first two papers in this thesis consider how scattering of sound can be measured, and how this can be used to measure mass fractions. The ideas are verified with experiments.

The third paper is on optimal experimental design. The problem is selecting suitable experiments from a large candidate set. We present a new algorithm for generating optimal designs.

The methods in the first two papers can be extended to incorporate more of the underlying physics, as well as using more sophisticated multi-dimensional signal processing techniques.

Contents

Preface

When I first started as an undergraduate student here in Luleå a few years ago, I had no plans of becoming a PhD student. On the other hand, I had not decided *not* to continue either. I just played along and now I am almost half-way through it, as it feels, more or less by accident. Who knows, maybe I will quit school someday.

However, the work that resulted in this thesis would not have possible without the help of a lot of people. First of all I would like to express my sincere gratitude towards my supervisor Anders Grennberg, who gave me the opportunity to proceed as a PhD student. Without his trust and inspiring ideas I would never have taken this challenging road. I would also like to thank Professor Jerker Delsing for all his help, and most of all, for hiring me in the first place. Generous grants from the *Swedish Research Council for Engineering Sciences* (TFR) is also gratefully acknowledged.

An interesting effect of ending up in the academic business was that my father, who is a professor in organic chemistry, finally came to me for help with a scientific problem. I never told him how proud I was, but now when it ended up being one of the papers in this thesis, I am even more glad he did. Thank you Dad!

Another important thing to mention is the inspiring environment that the other people at the department provided. Especially the other PhD students in my group and, of course, my friends Frank and Rickard at the division of Signal Processing. Thank you all!

I almost forgot to mention my close friend, Magnus Lundberg, who is more or less to blame for making me interested in signal processing in the first place. I owe you one!

Luleå, December 1999

Johan Carlson

Chapter 1

Thesis Introduction

1 Background

Several important process industries have different kinds of multiphase flows in their processes. A common problem is the need to measure different parameters in multiphase flows, in order to control and optimize the industrial processes. During the past decade measuring multiphase flows received a lot of attention from the scientific community. The main reason is that accurate measurement techniques are lacking, even for very limited applications.

Due to this, a research project was started associated to ProSA, the Centre for Process and System Automation. The long term goal of the research is to establish an ultrasonic measurement technique for multiphase flows, capable of measuring:

- Total volume flow.
- Mass fraction and mass fraction velocities of particles, fibers, and bubbles.
- Particle size distributions.

We are primarily interested in measuring the parameters of two types of multiphase flows:

- Iron ore slurry.
- Paper fiber suspensions.

These are homogeneous multiphase fluids having water as bulk fluid and solid particles, fibers and/or gas bubbles as the other phases. Often the suspensions have low concentration. In this thesis, focus has been on iron ore slurries and other mixtures where the particles can be considered spherical. In the case of paper fiber suspensions, the particles are more rod-shaped. This case has been investigated in another ProSA project, and results are presented in [1].

2 Measuring Multiphase Flows

The measurement of multiphase flow is, to say the least, difficult. This is obvious when looking into the huge varieties of multiphase flows around in industry. In general it is of

interest to measure the mass flow $\dot{m}$:

$$\dot{m} = \sum \dot{m}_i, \tag{1}$$

where $\dot{m}_i$ is the mass flow of each of the phases. To be able to handle the problem a decomposition of the flow into different parts could be a fruitful way. This description is by no means complete but probably usable for a large number of multiphase flow situations.

We distinguish between two multiphase flow types. Firstly, one where we have one major phase, the main bulk flow, into which the other minor phases flow are *mixed*. Secondly, we have a situation where the present phases do have a approximately equal volume or mass relations. From a measurement point of view the following decomposition is useful for the first type of flows:

- Measure the main bulk flow, which can be either a gas phase flow or a liquid phase flow.
- Measure the minor phase/phases flow.

To be able to find the combined mass flow we have to find one or more properties of the minor phase. These are:

- The average velocity
- The concentration
- The density or composition.

From these properties the minor phase is possible to calculate. For the first type of multiphase flow, several approaches to its measurement are possible. One possibility is by combining a bulk flow measurement technique with one or more techniques to obtain the necessary information of the minor phase. Another is the use of sophisticated instrumentation like NMR (see below) to obtain all information using the same basic technology.

The second situation, with two or more phases of equal volume or mass fraction ratio, is even more complicated. First we can face a number of different flow regimes, like stratified flow, slug flow, etc. A good measurement strategies can be to ensure that the multiphase flow meter always operates under a known flow regime, thus enabling the use of a techniques applicable to one flow regime. If the flow regime is unpredictable, very few choices for reasonable flow measurements remain.

There are techniques available today for online measurement of bulk mass flow, that is $\dot{m}$ in equation (1). One example the coriolis mass flow meter [2]. The coriolis mass flow meter works well even for some multiphase flows. Another approach is to measure flow velocity and density, and combine the results to obtain the bulk mass flow. Methods for measuring density of one phase flows are also available. The density probe presented in [3] uses the attenuation and transit time of pulsed ultrasound to measure the density. For one phase flows, there are a number of methods to measure the flow velocity, some intrusive and some not.

Measuring the minor phases is a somewhat more difficult problem. This involves measuring mass fractions, mass fraction velocities, and possibly also particle size distributions. A common method to measure bubble size distributions is to use a two point resistivity probe. This probe consists of two needles at a fixed distance, and the measured resistance between them depends on the phase (gas or liquid). A non-intrusive approach for bubble size distribution measurement is the ultrasonic doppler technique presented by [4]. For other multiphase flows, particle size distributions are often determined by sieving of samples taken from the flow.

Although many of the properties of multiphase flows can be measured one by one, some of them online, there are currently no method available that can measure all of them. If a flow consists of several phases it is desirable to be able to measure mass fractions and mass fraction velocities for all phases. In our project, the flow consists of iron ore particles, water, and possibly air bubbles.

The following subsections give a short overview of different methods currently available for multiphase flow measurement, such as:

- Optical methods
- Impedance methods
- Nuclear magnetic resonance imaging (NMR)
- Computerized tomography
- Ultrasonic techniques

2.1 Optical Methods

In general, optical probes can only be used in transparent systems, thus excluding the use in iron ore slurry and paper fiber suspensions. In order to be able to discriminate between phases the contact between the probe and the particles or gas bubbles must be very good. Also, if gas bubbles or particles are too small, the probe will not be able to detect changes in the flow. Because of difficulties in resolving the signals from solid particles and bubbles, it is considered difficult to use optical probes in three phase systems [5].

For liquid/gas mixtures, where the concentration of the gas phase is small, and the bubble size is fairly large, there are optical methods that can be used. The probes exploit differences in refraction index between the phases. De-Lasa et al. [6] presented a method where they used a U-shaped optic fiber (see figure 1). The curvature of the U is large enough for the angle incidence to be larger than the angle of total reflection for gas bubbles. At the same time the radius must be small enough for the angle of incidence to be smaller than the angle of total reflection when the fiber is in contact with water. With this setup, light will be lost in liquid (water), but conserved in gas.

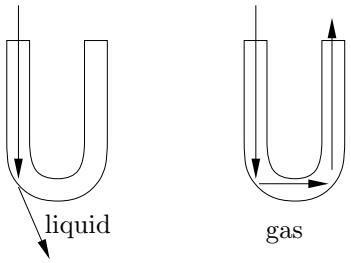

Figure 1: Optical U-shaped probe used for volume fraction measurements in gas/liquid mixtures

2.2 Impedance Methods

Probes measuring electrical impedance can be based on either conductive, resistive, or capacitive effects. A conductivity probe (see figure 2) makes use of the difference in

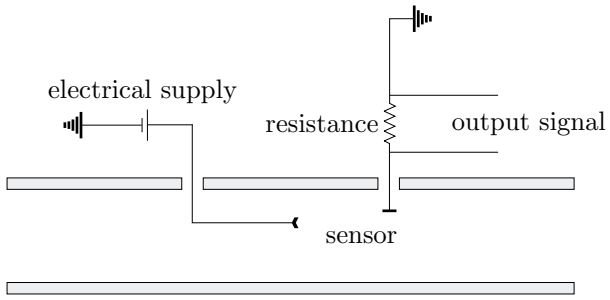

Figure 2: Conductivity probe used to measure differences in conductivity between phases.

conductivity of the phases [7]. These probes are best suitable for gas/liquid mixtures, but have recently been applied to oil/water emulsions [8]. Resisitivity probes sense the variation in resistance between two electrode. They are more suitable for measurement of solid/liquid mixtures. Capacitance probes (see figure 3) measures the difference in

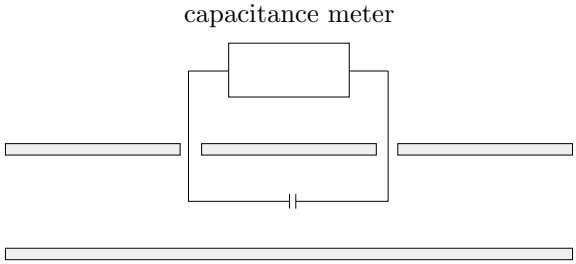

Figure 3: Capacitance probe used to measure differences in dielectric constant between phases.

dielectric constant between the phases [9, 10]. These are also mostly used in solid/liquid mixtures and in three phase systems.

2.3 Nuclear Magnetic Resonance Imaging

Nuclear magnetic resonance (NMR) imaging is a non-invasive method based on the magnetic properties of the nuclei of the atom. Each nucleus has a spin quantum number characterizing the stable ground state of the nucleus. Associated with the spin of the nucleus, there is an angular momentum and a proportional magnetic dipole moment, also known as the gyromagnetic ratio. In an NMR experiment, the atoms interact with a static magnetic field.

NMR imaging has received a lot of attention due to the advances made in medical imaging. NMR is also useful in many non-medical applications, for example in measuring flow velocity in paper fiber suspensions [11]. Some recent results from applying NMR imaging to multiphase flow measurements can be found in [12]. However, if the particles in a multiphase flow are magnetic, NMR will not work. Unfortunately this is the case for iron ore slurry.

2.4 Computerized Tomography

Although techniques based on probes are accurate and give good time resolution, they only measure local properties of the flow. In order to obtain information of the entire flow field, the probes have to be moved through the volume. With computerized tomography an image of a cross section of the flow is obtained. This technique has recently been used to obtain parameters such as void fraction and distribution in two phase flow systems [15, 16].

Tomography based on penetrating radiation of for example X-rays or γ-rays has been used in medical applications since the mid-50's to locate or examine a specific organ without opening the patient. Sometime in the early 70's, the methods for inverse imaging developed to be usable in practice. In medical imaging, techniques involving penetrating radiation are placed in two categories: Attenuation techniques and emission techniques. These will be described in the following two sections. Some of these techniques have recently been adopted to engineering application, such as multiphase flow measurements.

2.4.1 Attenuation Techniques

Attenuation techniques involves an external source of radiation, usually X-rays or γ-rays, but sometimes also ultrasound. X-rays and γ-rays are often used in a through-transmission mode as in figure 4a and b. A scanning system measuring γ-ray attenuation in a two-phase flow was presented by Swift, et al. [17]. A recent method using high speed S-ray tomography for measuring void fraction distribution was presented in [13]. Another recent method for measuring volume fractions and velocity profiles in two-phase flows was presented in [14]. In medical ultrasound, an array measuring the back-scattering of ultrasound is often used (see figure 4c). High frequency ultrasound is heavily attenuated in air, which makes a rotating setup difficult. In fan beam tomography (see figure 4a), one source that radiates in a fan beam pattern is used. The attenuation is then measured using an array of receivers. The procedure is then repeated for different angles (the whole setup is rotated around the sample) to obtain a large set of projections. These projections

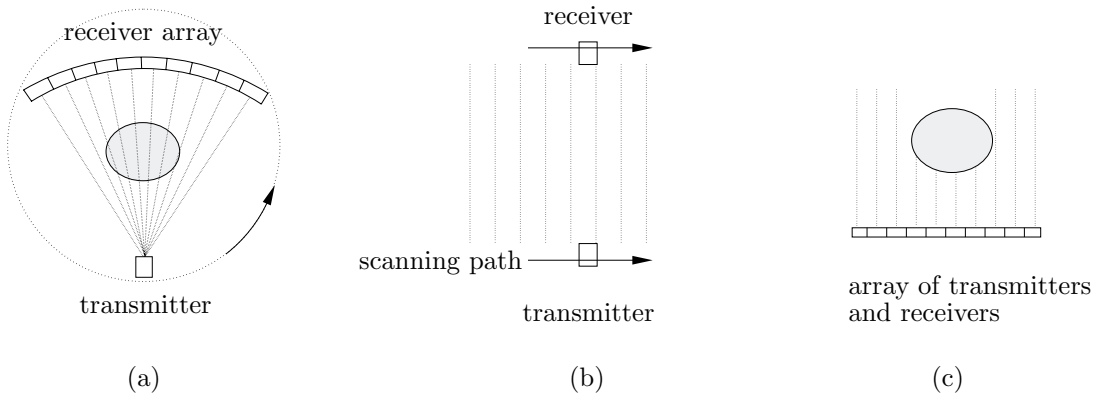

Figure 4: (a)- Fan beam tomography, (b)- Line scanning techniques, (c) - Phased array

can then be used to reconstruct an image of the sample object [18]. Figure 4c) shows a phased array. The different element of the array can be activated in such order to shape the transmitted lobe. This is not not used in tomography, but is a common use of ultrasonic arrays in medical imaging.

2.4.2 Emission Techniques

In for example Positron emission tomography (PET), the source is not externally positioned. In emission techniques, the radiation originates from radioactive tracers that decay with the emission of positrons.

In a multiphase flow, emission techniques can be used by labeling one of the phases with radioactive tracers. The amount of emitted γ-rays can then be used to monitor the fraction of that particular phase.

2.5 Ultrasonic Techniques

Some recent reviews [19, 20] position ultrasound as a technique that is non-invasive, has high temporal resolution, and that can penetrate opaque, highly concentrated mixtures.

During the nineties, a series of papers on ultrasound techniques for multiphase flow measurement and characterization has been published. Atkinson and Kytömaa have studied how wave speed and attenuation of ultrasound are affected by multiphase flows [21], and what limitations there are to ultrasound methods [22].

Sound propagation phenomena, such as attenuation and speed of sound, will be affected by the composition of the flowing medium. The transmitted ultrasound signal will therefore be modulated by a multiphase flow. Several physical processes are involved in such modulation, for example:

- Scattering effects,
- dispersion effect,
- viscosity effects,

- molecular effects,
- resonance effects.

In the papers in this thesis, focus is mainly on the effect of scattering, and how to measure and model this. Given some knowledge about the particles, and assuming they can be regarded as spheres, it is possible to model the scattering [23, 24, 25]. It is of interest to model how scattering affects both the shape (amplitude, and phase) of the signal, and the spread within the suspension.

The idea is to use array signal processing techniques to be able to investigate spatial effects of scattering and other phenomena. The use of receiver arrays also makes it possible to measure relative effects, reducing the errors caused by changes in the surroundings.

3 A Few Words on Experimental Design

In any experimental science, planning of experiments is crucial. Poorly designed experiments can give misleading results. In any experimental system, a number of variables might influence the results. Varying one at a time is generally a bad idea, especially if there are interaction effects between the variables. Considering all variables simultaneously at the planning stage needs both some understanding of the underlying physical problem, and about experimental design principles.

When the objective is to find out how different variables affect the outcome of experiments, a commonly used design strategy is something called two-level factorial designs [26]. In a two-level factorial design each of the N variables in the model is assigned two levels, one high and one low. A table of all possible combinations of the variable settings is then constructed, resulting in 2^N experiments. The construction of such a table is easily automated, but it is important that the order in which the experiments are actually conducted is randomized. This will ensure that systematic variations due to factors out of control of the experimenter, will appear as noise. Otherwise, there is a risk that for example changes in the experimental environment will. If this is done, the effect of each of the variables, as well as interaction effects between two or more variables, can be estimated after the experiments have been conducted. Factorial designs can also be constructed with more than two levels for each variable, but the number of experiments that has to be conducted will increase rapidly. A more detailed description of the principles behind factorial designs can be found in the book by Box, *et al.* [27].

The third paper in this thesis is a result of an idea that professor Rolf Carlson[1] brought to us. When an experimenter is faced with a new experimental situation, where nothing or little is known about the underlying model, it is desirable to perform a so-called screening experiment. The objective of a screening experiment is to cover as much as possible of the total experimental variation with a small number of experiments. Hopefully, the results of these experiments will indicate how further experiments should be designed. In a situation where little is known, a common model assumption is that

[1]Department of Chemistry, Faculty of Science, University of Tromsø, Norway

the outcome can be expressed as a second order Taylor approximation

$$f(x_1, x_2, ..., x_N) \approx \beta_0 + \sum_{i=1}^{N} \beta_i x_i + \sum_{i=1}^{N} \sum_{j=1}^{N} \beta_{ij} x_i x_j, \quad (2)$$

where $x_1, x_2, ..., x_N$ are the experimental variables, and the regression coefficients $\{\beta_{n,m}\}$, are to be estimated using a least squares method.

Given a number of variables that are believed to affect the outcome of the experiments, we can construct a full factorial design with all combinations of the variable settings. The problem arises when each of the variables can have many values, because the experimental design will become much too large to be practical. When planning a screening experiment, it is also difficult for the experimenter to judge which levels that are representative, which would otherwise reduce the number of possible combinations. To solve this problem, we needed another approach. There is a field in experimental design called *optimal design*, introduced by Jack Kiefer [28, 29], where these types of problems are treated. In the book by Fedorov [30], some principles of optimal designs are described in detail.

The idea was that, given a number of experiments we want to conduct, and the set of all possible experiments (i.e. the full-factorial design), it should be possible to select the subset that covers as much as possible of the total variation, and at the same time minimizes the variance of the estimated model coefficients in equation (3). This would give the experimenter a good idea of which variables should be in the model, and also give indications of a region of interest, where further experiments can be performed, using a conventional design strategy.

Paper C in this thesis contains a more detailed problem formulation as well as a new algorithm for generating such an optimal design.

In the multiphase flow project, the number of possible experiments rapidly increases if we want to examine many experimental variables. Because of this, we plan to use the proposed strategy to design our experiments.

4 Summary of Contributions

This section will give a brief summary of the contributions of the papers in this thesis. The papers A and B are on multiphase flow measurements, and paper C is on optimal experimental design.

4.1 Paper A - Multiphase Flow Characterized by Scattering of Ultrasound

When ultrasound propagates through a suspension of water and solid particles, the sound is scattered by the particles. The idea behind this paper was to investigate if a simple multi-path propagation model could be used to simulate the propagation through such a suspension.

The experimental setup consisted of one transmitter and one receiver, mounted on opposite sides of the suspension. The assumption was that the received ultrasound pulses

can be modeled as a sum of delayed and attenuated versions of the transmitted pulses. The particles used in both simulations and experiments were large compared to the wavelength of the sound.

The experimental results agree well with the simulations, at least for low concentration of particles.

4.2 Paper B - Ultrasonic Measurements of Particle Concentration in a Multiphase Flow

This paper is a first attempt to use a multi-dimensional techniques to measure particle concentrations in multiphase flows. The idea is that when the sound is scattered by particles, the shape of the transmitted energy lobe will change. One way to measure this is to use several receivers mounted close to each other. In this paper we used two receivers and used the relative difference in received energy to measure the change of the lobe.

The results showed that for iron ore particles, this method can be used to measure the mass fraction of particles within $\pm 1\%$. The iron ore particles were much smaller than the wavelength of the ultrasound, as compared with the opposite relationship in paper A.

4.3 Paper C - A Fast Algorithm for Generating Optimal Designs for Regression Problems

This paper is on a different topic, and the idea originally came from the area of organic synthesis. When an experimenter is confronted with a new experimental situation and the objective is to examine which variables that affect the outcome of the experiment, and how. Each of the variables can often take on several different values, and when the number of variables increases, the number of possible experiments becomes prohibitively large.

The problem addressed in this paper is that, if a given number of experiments are to be performed, typically much less than the number of possible experiments, which should these experiments be?

The problem is solved by first assuming multiple regression model for the outcome of an experiments, and then select the experiments that minimize the variance in the estimated model parameters.

5 Conclusions

The result in paper A shows that it is possible to model the effect of multi particle scattering of ultrasound in some multiphase flows, using a simple model of multi-path propagation. The simulations indicate that the received ultrasonic pulse can be modeled as the sum of several delayed and attenuated versions of the transmitted pulse. This way, we model the temporal effect of scattering.

In paper B, we used a very simple approach to measure how the transmitted energy is scattered over a wider area when the mass fraction of particles was increased.

By using an array of receivers, together with a multi-path propagation model, it should be possible to obtain even more information about the suspension.

6 Future Work

Papers A and B both show promising experimental results. These results have to be investigated further. The multi-path propagation model in paper A will be extended to model the scattering based on the physics of the suspension and the transmitting transducer, instead of calibrating all model parameters.

Some of the problems have been that the experimental environment changes during measurements. Depending on what we measure, amplitude changes or phase changes, variations in ambient temperature, for example, can cause problems. In paper B we use a two-element receiver, and when signals from both of them are combined, the sensitivity to ambient changes decreases. We are currently modifying and extending our experimental equipment in order to be able to use a larger array of receivers. Now we can use only four receivers, but after the changes, we will be able to use an array with up to sixteen receiver elements.

References

[1] Löfqvist, T. *Ultrasonic Measurement Technology for Characterization of Paper Fibre Suspensions.*, PhD thesis, ISSN:1402-1544, Luleå University of Technology, Sweden, 1999.

[2] Spitzer, D. W. (editor), *Flow Measurement.* Instrument Society of America, Research Triangle Park, NC, 1991.

[3] van Deventer, J. A., and Delsing, J., "An Ultrasonic Density Probe," in *Proc. 1997 IEEE Int. Ultrasonics Symp.* ,pp. 871-875, 1997.

[4] Hilgert, W., and Hoffman, H., "Characterization of Gas Phase Flow in Bubble Columns at Low Superficial Gas Velocities With the Aid of Ultrasonic Doppler Technique," *Ger. Chem. Eng.*, 9, pp. 180-190, 1986.

[5] Euzen, J. P., Trambouze, P., and Wauquier, J. P., *Scale-Up Methodology for Chemical Processes*, Editions Technip., Paris, 1993.

[6] De-Lasa, H., Lee, S. L. P., and Bergougnou, M. A., "Bubble Measurement in Three Phase Fluidized Beds Using U-shaped Optical Fiber," *Can J. Chem. Eng.*, 62, pp. 165-169, 1984.

[7] Nasr-El-Din, H., Shook, C. A., and Colwell, J., "A Conductivity Probe for Measuring Local Concentrations in Slurry Systems," *Int. J. Multiphase Flow*, 13, pp. 365-378, 1987.

[8] Liu, Ximgbin, et al. "A Novel Impedance Sensor for Measuring Water Fraction in An Oil-Water Two Phase Flow," in *Proc. of the 9th Int. Conf. on Flow Measurements, FLOMEKO'98,* (Lund, Sweden), pp. 273-278, IMEKO 1998.

[9] Riley, A. C. and Louge, M., "Quantitative Capacitance Measurements of Voidage in Gas-Solid Flow," *Part. Sci. Tech.*, 7, pp. 51-59, 1989.

[10] Louge, M. and Opie, M., "Measurement of the Effective Di-electric Permitivity of Suspensions," *Powder Technology*, 62, pp. 85-94, 1990.

[11] Li, T.-Q., et al. "Velocity Measurements of Fiber Suspensions in Pipe Flow by the Nuclear Magnetic Resonance Imaging Method," *Tappi J.*, 77(3), March 1994.

[12] Tokarczuk, P. F., Sanderson, M. L., and High, G. "The Application of Nuclear Magnetic Resonance (NMR) to Multiphase Flow Metering," in *Proc. of the 9th Int. Conf. on Flow Measurements, FLOMEKO'98,* (Lund, Sweden), pp. 291-296, IMEKO 1998.

[13] Harvel, G. D., Hori, K., Kawanishi, K., and Chang, J. S., "Cross-sectional void fraction distribution measurements in a vertical annulus two-phase flow by high speed x-ray computed tomography and real-time neutron radiography techniques," *Flow Measurement and Instrumentation*, vol. 10, no. 4, pp. 259-266, 1999.

[14] Lucas, G. P., Cory, J., Waterfall, R. C., Loh, W. W., and Dickin, F. J., "Measurement of the solids volume fraction and velocity distributions in solids-liquid flows using dual-plane electrical resistance tomography," *Flow Measurement and Instrumentation*, vol. 10, no. 4, pp. 249-258, 1999.

[15] Ashrafi, M. E. H. and Tuzun, U., "A Tomographic Study of Viodage Profiles in Axially Symmetric Granular Flows," *Chem. Eng. Sci.*, vol. 25, no. 3, pp. 373-380, 1993.

[16] De Vuono Schlosser, P. A., Kulacki, F. A., and Munshi, P., "Design of an Isotopic CT Scanner for Two Phase Flow Measurements," *IEEE Trans. on Nucl. Sci.*, vol. NS-27, no. 1, pp. 814-820, 1980.

[17] Swift, W. L., Dolan, F. X., and Runstadler, P. R., "A Scanning Gamma Ray Attenuation System for Void Fraction Measurements in Two-Phase Flow," in *Measurements in Polyphase Flows, Proc. of the Winter Annual Meeting of ASME,* San Fransisco, pp.25-35, 1978.

[18] Herman, G. T., *Image Reconstructions From Projections - The Fundamentals of Computerized Tomography.* Academic Press, 1980.

[19] Whitaker, T. S., "A Review of Multiphase Flowmeters and Future Development Potential," in *Flow Measurement: Proceedings of the 6th Int. Conf. on Flow Measurement FLOMEKO'93.* (Seoul, Korea), pp. 628-634, Oct. 1993.

[20] Chaoki, J., Larachi, L., and Dudoković, M. P., *Non-Invasive Monitoring of Multiphase Flows.* Elsevier, 1997.

[21] Atkinson, C. M. and Kytömaa, H. K., "Acoustic Wave Speed and Attenuation in Suspensions," *International Journal of Multiphase Flow*, vol 18, no. 4, pp. 577-592, 1992.

[22] Atkinson, C. M. and Kytömaa, H. K., "Acoustic Properties of Solid-Liquid Mixtures and the Limis of Ultrasound Diagnostics - I: Experiments," *Journal of Fluids Engineering*, vol 115, pp. 665-675, 1993.

[23] Allegra, J. R. and Hawley, S. A., "Attenuation of Sound in Suspensions and Emulsions: Theory and Experiments," *The Journal of the Acoustical Society of America*, vol 51, no. 5, pp. 1545-1564, 1972.

[24] Povey, M. J. W. *Ultrasonic Techniques for Fluid Characterization.* Academic Press, 1997.

[25] Lynnworth, L. C. *Ultrasonic Measurements for Process Control.* Academic Press, 1989.

[26] Yates, F. *The Design and Analysis of Factorial Experiments*, Bulletin 35, Imperial Bureau of Soil Science, Harpenden, Herts, England, Hafner (Macmillian), 1937.

[27] Box, G. E. P., Hunter, W. G., and Hunter, J. S. *Statistics for Experimenters.* John Wiley and Sons, 1978.

[28] Kiefer, J., "On the Nonrandomized Optimality and the Randomized Nonoptimality of Symmetrical Designs," *Ann. Math. Stat.*, 29, 675-699, 1958.

[29] Kiefer, J. and Wolfowitz, J., "Optimum Designs in Regression Problems," *Ann. Math. Stat.*, 30, 271-294, 1959.

[30] Fedorov, V. *Theory of Optimal Experiments*, Academic Press, 1972.

Paper A

Multiphase Flow Characterized by Scattering of Ultrasound

Authors:
Johan Carlson, Anders Grennberg, and Jerker Delsing

Edited version of paper originally published in:
Proc. of the 9th Int. Conf. on Flow Measurements, FLOMEKO'98, (Lund, Sweden), pp 493-498, IMEKO 1998.

Multiphase Flow Characterized by Scattering of Ultrasound

Johan Carlson, Anders Grennberg, and Jerker Delsing

Abstract

In this paper, we present and verify a simple mathematical model of the scattering of ultrasound by particles in a multiphase flow.

We show that a *line-of-sight* model can be used to describe how the multi-path propagation of ultrasound in a dilute suspension of glass spheres and water affects the waveform. Simulation results agree with measured data for particle concentrations up to 3 percent.

Furthermore, the simulations and experiments indicate that there are two main effects affecting the signal waveform; the shadowing of the direct wave between transmitter and receiver, and multi-path propagation. For small particles, the multi-path propagation is the largest effect, while the attenuation of the direct wave increases for larger particles. We see that the multi-path propagation affects the tail of the pulse, while the attenuation of the direct wave mainly affects the first two maxima. The relationship between these two effects can therefore be used to characterize a multiphase suspension.

1 Introduction

The long-term goal of our project is to develop a non-invasive multiphase flow metering methodology for measuring bulk flow velocity, mass fractions, and mass fraction velocities in dilute multiphase flows. Important areas of application are, oil and gas, paper pulp, and mining industry. A good overview of what has been done in this area can be found in the book by Chaoki, *et al.* [1] and in the review article by Whitaker [2]. Our basic idea is to use some established method for measuring the bulk flow velocity (see for example the sing-around flow meter described in [3]), and then use through-transmission ultrasound to determine mass fractions and mass fraction velocities. In this paper, we characterize a multiphase flow by examining how scattering affects the received signal waveform.

When transmitting ultrasound through a multiphase medium containing solid particles, the sound waves are scattered and attenuated. In this paper, we present and verify a mathematical model that qualitatively describes how scattering affects the waveform of ultrasonic pulses. The idea behind the model is that the received ultrasonic signal can be written as the sum of a direct wave between the transmitter and the receiver, and scattered waves.

2 The Multi-path Propagation Model

Under certain conditions, scattering occurs when sound waves are obstructed by particles. As a rule of thumb (see for example [4], chapter 8) we can assume that scattering occurs if the condition in equation (1) is satisfied.

$$\frac{2\pi}{\lambda}a \gg 1, \tag{1}$$

where λ is the wavelength of the sound and a is the radius of the scattering particle.

Since the theory of scattering is very complex, we will derive a simplified mathematical model, that qualitatively describes the effect of scattering on the waveform of a received ultrasonic pulse. Figure 1 illustrates the general idea of the *line-of-sight* scattering model. Assume that waves transmitted from the transducer are scattered by N spherical particles

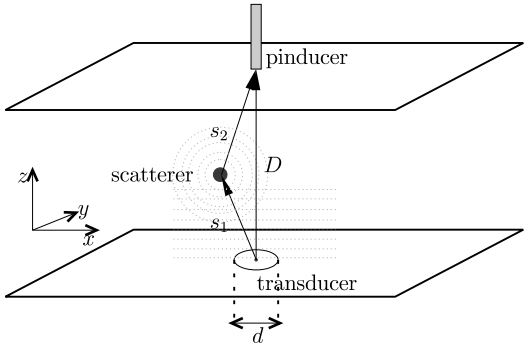

Figure 1: Line-of-sight model for single scattering by a spherical particle.

as in figure 1. In this case the received pulse, $y(t)$, can be regarded as the sum of delayed and attenuated versions of the transmitted pulse, $p(t)$. Equation (2) is a mathematical representation of this idea

$$y(t) = \alpha_0 p(t) + \sum_{n=1}^{N} \alpha_n p(t - \tau_n), \tag{2}$$

where α_0 is the attenuation of the direct wave, $\{\alpha_1, \alpha_2, \ldots, \alpha_N\}$ is the attenuation coefficients for the N scatterers, $p(t)$ is the transmitted pulse, and τ_n is the time delay corresponding to the increase in distance caused by scatterer n. The attenuation coefficients depend on several factors, for example the position of the scatterer and the relationship between wavelength and particle size.

We assume that a particle will affect the received signal if it is located somewhere in the cylinder with the transmitting transducer as base, and with height D (as defined in figure 1). Figure 2 supports this, since we see that most of the received energy is located in that region.

If particle n is located at $(x_n,\ y_n,\ z_n)$ somewhere in this volume, the propagation distance $s_1 + s_2$ can be expressed as

$$s_n = \sqrt{x_n^2 + y_n^2 + z_n^2} + \sqrt{x_n^2 + y_n^2 + (D - z_n)^2} \tag{3}$$

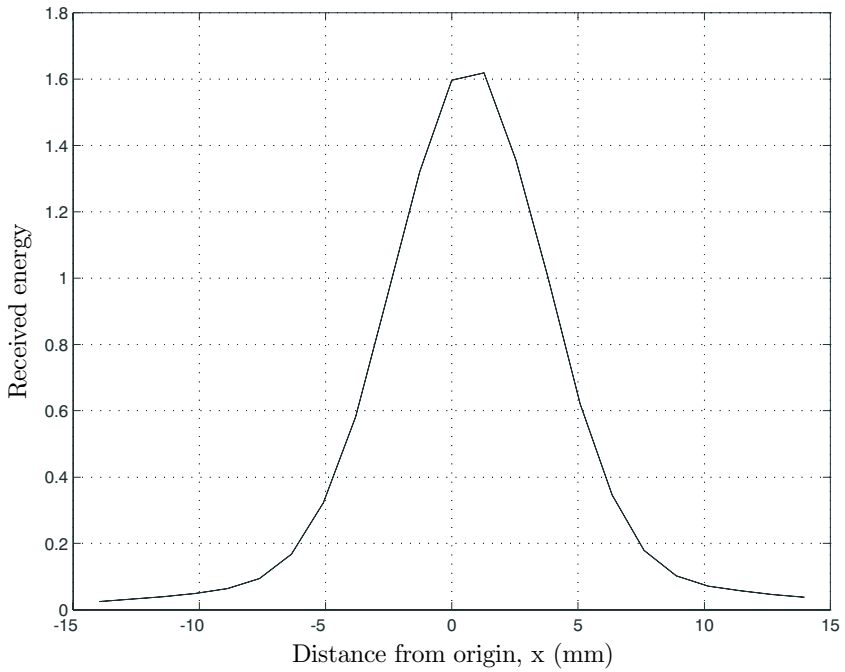

Figure 2: Received energy in the region around the origin, measured in pure water. The diameter of the transmitting transducer was 14 mm, and the distance between transmitter and receiver was 145 mm.

where we for simplicity assume that x_n and y_n are uniformly distributed over the interval $\left[-\frac{d}{2}, \frac{d}{2}\right]$ and that z_n is uniformly distributed over the interval $[0, D]$.

Using the distances s_n from equation (3), we obtain the corresponding time delays τ_n as

$$\tau_n = \frac{s_n(x_n, y_n, z_n) - D}{v} \tag{4}$$

where v is the speed of sound and D is the propagation distance of the direct wave.

For different relationships between particle size and wavelength, the energy is scattered differently in space. For simplicity we assume that the energy spreads spherically from the scatterer. We also assume the no energy is absorbed by the scatterer. Thus, the attenuation coefficient for each scattered pulse can be approximated to be

$$\alpha_n = \frac{K_2}{s_{n2}^2}, n \geq 1 \tag{5}$$

where s_{n2} is the distance between the n:th scatterer and the receiver and K_2 is some constant (to be determined experimentally). If no particles shadow the direct wave between transmitter and receiver, the attenuation of the direct wave is generally very small compared to the attenuation of the scattered waves. There are cases, however, when no direct wave is present, because some particles shadow the propagation path. In order to keep the model simple, we assume that the amount of received energy is proportional to the area of the receiver which is not shadowed. This leads to the following

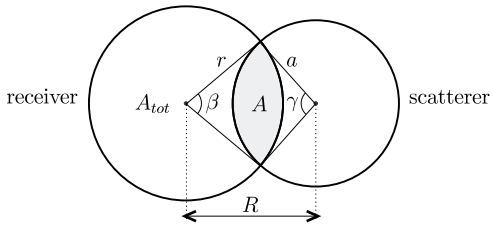

Figure 3: Situation where the scatterer shadows the receiver.

expression for α_0.

$$\alpha_0 = K_0 \left(1 - K_1 \frac{A}{A_{tot}}\right), \tag{6}$$

where K_0 is a constant corresponding to the attenuation of an undisturbed wave, K_1 is a constant corresponding to the amount of energy lost by shadowing, and A/A_{tot} is the ratio of the shadow to the receiver area. If there is only one scatterer shadowing the receiver, we have the case illustrated in figure 3. If the scatterer and the receiver partially overlaps, that is $\min(r, a) < R < r + a$, the area of the intersection, A, is given by

$$A = \frac{r^2}{2}(\beta - \sin\beta) + \frac{a^2}{2}(\gamma - \sin\gamma). \tag{7}$$

where, by the law of cosines,

$$\beta = 2\cos^{-1}\left(\frac{r^2 + R^2 - a^2}{2aR}\right) \tag{8}$$

$$\gamma = 2\cos^{-1}\left(\frac{a^2 + R^2 - r^2}{2aR}\right) \tag{9}$$

If, however, the receiver is totally shadowed or, if the scatterer is smaller than the receiver, we have a maximum shadowing area, given by

$$A = [\min(a, r)]^2 \cdot \pi \tag{10}$$

If there are more than one scatterer shadowing the receiver, the expression for A, becomes more complicated. For simplicity we sum the contributions of each scatterer, making sure that the total shadowed area is not greater than the receiver area.

3 Experiments

In this section, we first describe the experimental setup and the equipment we used, followed by a brief description of the analysis tools used to process the collected data. Finally, we describe how the computer simulations of the model in section 2 was made.

3.1 Experimental Setup

In order to verify the model, we prepared suspensions of glass spheres and water. The glass spheres had an average radius of 1 mm, which, according to equation (1), should be enough for scattering to be present, since the transmitting transducer had a center frequency of 3 MHz. The outer diameter of the transducer was 14 mm. We prepared suspensions with concentrations of 1, 2, and 3 percent (by volume). The suspensions were enclosed in the suspension tank depicted in figure 4.

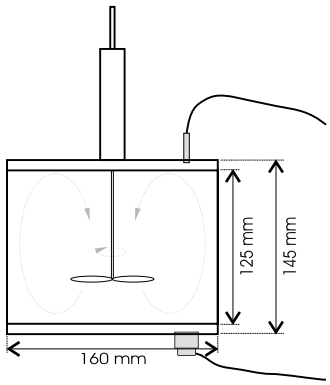

Figure 4: Suspension tank used in the experiments.

The receiver was a VP-1093 pinducer[1] with a 10 MHz input bandwidth and a crystal radius of 1 mm. The receiver and transmitter was centered.

For each concentration, 100 pulses were measured. We noticed that there were small time delays between the recorded pulses. We found that some of these delays came from triggering of the sampling equipment, and by increasing the sampling frequency this effect became smaller. We also found that when we increased the speed of the stirring equipment, the vibrations in the system increased. This may also cause time delays, since the distance between transmitter and receiver could change. If the observed time delays are the result of experimental errors, they have to be estimated and compensated for.

3.2 Estimating Time Delays

Whether or not the observed time delays were the result of experimental errors, they have to be estimated. To accomplish this, we used the algorithm by Grennberg and Sandell, presented in [5]. This is a more efficient method than an ordinary cross-correlation method, especially for estimating small time delays between narrowband pulses.

[1]The VP-1093 pinducer was manufactured by Valpey-Fisher Corp., 75 South Street, Hopkinton, MA 01748.

3.3 Sensitivity to Vibrations

In order to determine if the time shifts between recorded pulses were the results of mechanical disturbances, such as vibrations, we first estimated the time delays with respect to the first recorded pulse. Figure 5 shows the resulting histogram of the delays.

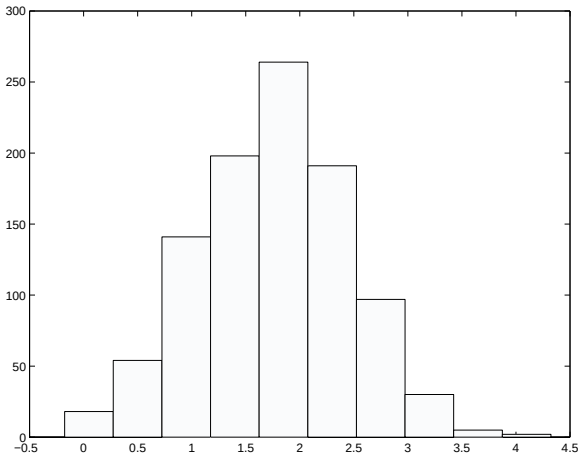

Figure 5: Distribution of estimated time delays, measured in water.

We note that the delays looks like they originate from a normal distribution. However, if the delays were due to mechanical disturbances, we would expect them to have zero mean. The observed bias can be explained by the fact that we estimated the delays relative to the first recorded pulse, and not to an *exact* measurement.

Now, if we assume that the delays are samples from a normal distribution with mean μ and standard deviation σ, a 95 percent confidence interval can be calculated. Since the mean and standard deviation are unknown, we first estimated these, using equations (11) and(12).

$$\widehat{\mu} = \frac{1}{N}\sum_{n=1}^{N}\theta_n, \tag{11}$$

$$\widehat{\sigma} = \left[\frac{1}{N-1}\sum_{n=1}^{N}\left(\theta_n - \widehat{\mu}\right)^2\right]^{1/2}. \tag{12}$$

The corresponding precision limits are then given by(see [6])

$$P_\theta = t_{N-1}\cdot\widehat{\sigma}, \tag{13}$$

$$P_{\widehat{\mu}} = t_{N-1}\frac{\widehat{\sigma}}{\sqrt{N}}, \tag{14}$$

where the t-distribution is used because $\widehat{\sigma}$ was estimated.

This means that, with 95 percent probability, the $\left[-P_\theta - P_{\widehat{\mu}}, P_\theta + P_{\widehat{\mu}}\right]$ will enclose the time delays.

To see whether or not the time delay corresponding to the precision limit $P_\theta + P_{\widehat{\mu}}$ is likely to come from vibrations, we calculated the change in distance between the transmitter and receiver this would require. The sampling time was $2 \cdot 10^{-9}$s and the speed of sound in water is around 1480 m/s. For the measurements shown in figure 5 the upper precision limit was determined to be 1.39 samples. Equation (15) gives the corresponding change in distance, ds.

$$\begin{aligned} ds &= \left(P_\theta + P_{\widehat{\mu}}\right) \cdot T_s \cdot v = \\ &= 1.39 \cdot 2 \cdot 10^{-9} \cdot 14804.0 \mu m \end{aligned} \tag{15}$$

For the case with 3 percent particle concentration, the corresponding distance would be 20 μm, assuming all time shifts come from distance changes.

As we see, the distance change required to cause these time delays is very small, and we conclude that it certainly could come from vibrations and other mechanical disturbances in the system. When we increased the particle concentration, we had to use a higher rotation speed, causing more vibrations. If we average the measured pulses directly, the time delays cause the signal waveform to be distorted.. Therefore, we first shift all measured pulses according to the estimated time delays, by using Lagrange's interpolation formula.

4 Results

After measuring all pulses, we simulated 100 pulses for each concentration. Based on the concentration, the position of a number of particles was generated, assuming that the particles were uniformly distributed in the sample volume. As input pulse to the model, we used an average pulse taken from measurements in pure water. The parameters, K_0, K_1, and K_2 in the model described in section 2 was then adjusted so that the average pulses from the measurements and simulations fit for the suspension with 1 percent of glass spheres. We then performed simulations for the other concentrations, but without changing any parameters in the model. Figure 6(a) shows the resulting average pulse after adjusting the model parameters. Figure 6(b) and (c) show how the model follows when concentration was increased to 2 and 3 percent, respectively. In this case the model parameters were set as $K_0 = 0.8$, $K_1 = 0.5$, and $K_2 = 6.5 \cdot 10^{-5}$. These values were chosen so that the model output and the measured pulses agree for 1 percent of glass spheres.We see that the agreement is very good for 1 and 2 per cent, but slightly worse for 3 percent of glass spheres. When deriving the model, we assumed that the sound is only scattered once during the propagation. When the concentration of particles increases, this assumption does no longer hold, and this could be what we see in figure 6(c). Figure 6 shows that the simulated signal waveform agrees with measured data, and in figure 7 we see that the average energy of the simulated pulses also agrees with measured data.

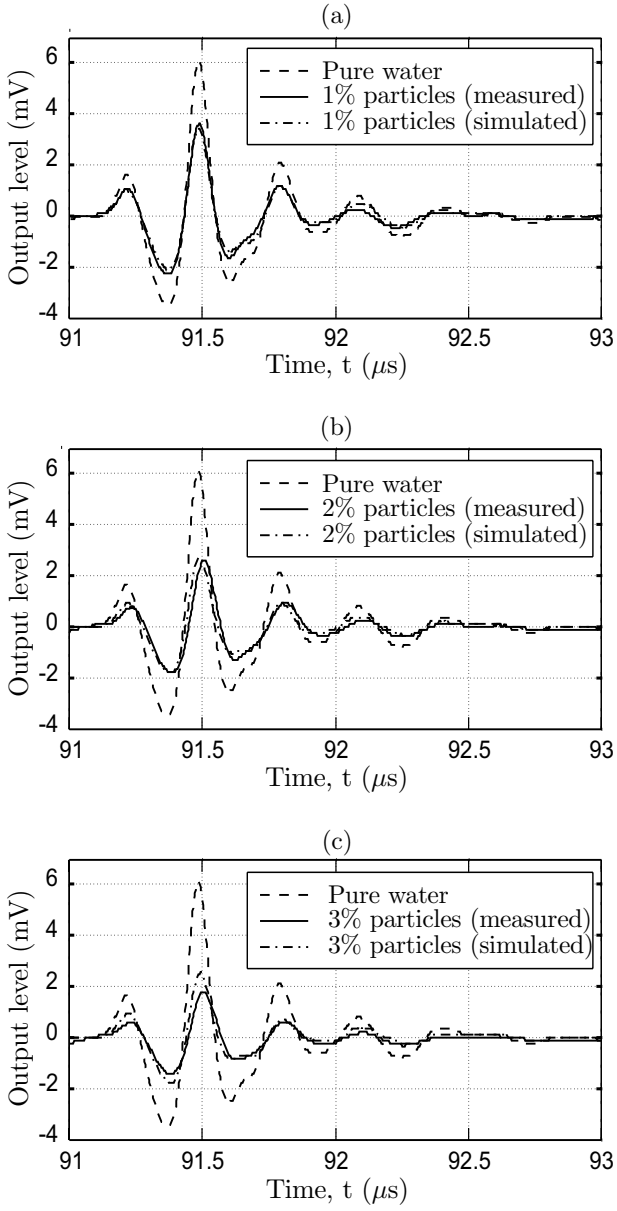

Figure 6: Comparison of averaged pulses

5 Conclusions

From the simulations we conclude that this model can be used to qualitatively describe the effect of scattering of ultrasound for this experimental setup. It is clear that the main effect is the shadowing of the direct wave between the transmitter and the receiver. The multi-path propagation is also significant to the change of waveform, and we can see that when scattering occurs, the variations in pulse energy increase towards the end of the pulse. For large particles, the shadowing of the direct wave is the main effect, while for smaller particles, the multi-path propagation increases, causing larger variations at the

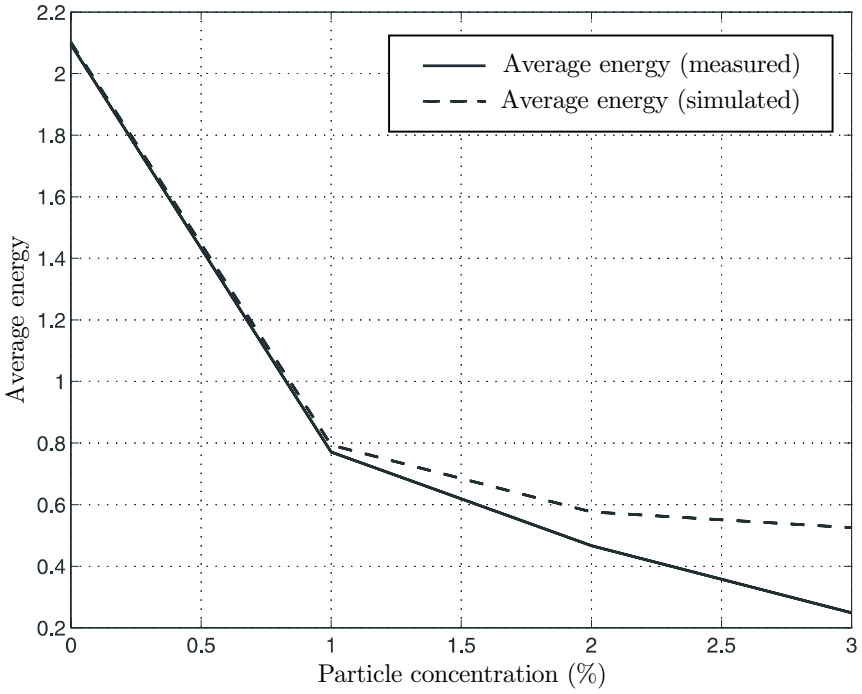

Figure 7: Average energy for measured and simulated pulses.

tail of the pulses. Thus, by studying the waveform of a received ultrasonic pulse, we can determine whether or not scattering has occurred, and by that draw conclusions about the particle size and attenuation. If the model is developed further, it is possible that the relationship between the damping of the first two maxima of the pulse and the increase of energy in the tail of the pulse can be used to determine volume fractions.

We also see from the simulations that the assumption that the sound is scattered only once, only holds for low particle concentrations.

References

[1] J. Chaoki, L. Larachi, and M. P. Dudoković, *Non-Invasive Monitoring of Multiphase Flows*. Elsevier, 1997.

[2] T. S. Whitaker, "A review of multiphase flowmeters and future development potentials," in *Flow Measurment: Proceedings of the 6th Int. Conf. on Flow Measurement, FLOMEKO'98*, (Seoul, Korea), pp. 628-634, Oct. 1993.

[3] J. Delsing, "A new velocity algorithm for sing-around type flow meters," *IEEE Trans. on Ultrasonics, Ferroelectrics, and Frequency Control*, vol 34, no. 4, pp. 431-436, 1987.

[4] P. M. Morse and K. U. Ingaard, *Theoretical Acoustics*. Princeton University Press, 1986.

[5] A. Grennberg and M. Sandell, "Estimation of subsample time delay differences

in narrowband ultrasonic echoes using the Hilbert transform correlator," *IEEE Trans. on Ultrasonics Ferroelectrics, and Frequency Control*, vol. 41, pp. 588-595, Sep 1994.

[6] H. W. Coleman and W. G. Steele Jr., *Experimentation and Uncertainty Analysis for Engineers.* Wiley Interscience, 1989.

Paper B

Ultrasonic Measurements of Particle Concentration in a Multiphase Flow

Authors:
Johan Carlson and Anders Grennberg

Edited version of paper originally published in:
Proc. of IEEE International Ultrasonics Symposium 1999, (Lake Tahoe, Nevada, USA), 1999. In print.

Ultrasonic Measurements of Particle Concentration in a Multiphase Flow

Johan Carlson and Anders Grennberg

Abstract

Non-invasive measurements of multiphase flows have several important applications in industry. In this paper we present a method that uses pulsed ultrasound and two small receivers to determine the mass concentration of iron ore particles in water.

The proposed method is based on the assumption that when ultrasound is transmitted through a scattering medium, the shape of the energy lobe changes. In this paper we use two receivers to monitor how the lobe changes.

We show with experiments how the proposed method can be used to determine particle mass fractions from 3 percent and up, with an accuracy of ± 1 percent of the mass fraction. In the experiments we used a 3 MHz transmitter and two receivers, one along the acoustical axis and the other 6mm off-axis, to measure the mass fraction of a polydisperse suspension of iron ore powder in water.

1 Introduction

In several industries, such as the oil and gas, paper pulp, and mining industries, multiphase flows are common. It is often of great importance to be able to measure the mass or volume fraction of the different phases in such flows. In the mining industry, for example, iron ore powder is transported using water, and there is a need of measurement techniques to monitor the particle mass fraction. There exists several methods for doing this, all with their drawbacks and advantages. Some methods are based on optical techniques, which requires the flow to be transparent, other methods are based on nuclear magnetic resonance or inductance/conductance measurements. If the medium is opaque or if the solid particles are magnetic, these methods all have their drawbacks. Also, X-ray techniques and other methods based on radioactivity are both expensive and can be hazardous to the environment. A good overview can be found in the book by Chaoki, *et al.* [1], and in the review article by Whitaker [2].

The long term goal of our research project is to develop a ultrasonic technique for measuring mass fractions and mass fraction velocities in multiphase flows. The use of ultrasonic techniques has several advantages. It does not require the medium to be transparent. Depending on the frequency, it can be used to monitor both liquid/solid flows and liquid/gas flows.

In this paper we present a method that can be used to measure particle mass fractions in i multiphase flow consisting of water and iron ore particles. The method is based on pulsed ultrasound and the fact that transmitted pulse is scattered by the solid particles

(see for example [3]). If we assume that the scattering results in a change of the shape of the lobe from the transmitting transducer, this change can be used to monitor concentration changes. If we calibrate the method for a given type of particles, the method can be used for online measurement of the particle mass fraction. The transmitted lobe can be measured by using an array of small receivers. In this paper we use only two receivers, and we show how the ratio of the energy received at the receivers can be used to estimate lobe changes.

2 Experimental Setup

All experiments were conducted in the suspension container depicted in figure 2. The bottom and the lid of the container is made of moulded plexiglass, which has acoustical characteristics similar to those of water. In order to reduce the influence of temperature

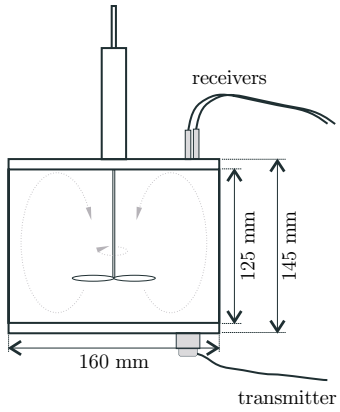

Figure 1: Suspension container used in the experiments.

fluctuations, the ambient temperature in the lab was controlled and lies within $\pm 1^{\circ}$ centigrade.

The transmitting ultrasound transducer, which had a center frequency of 3 MHz, was fixed to the bottom of the container, and the receivers[1] were mounted on the top. One of the receivers was centered relative to the acoustical axis of the transmitter, and the other receiver was mounted 6 mm away from the center. The received signals were connected to a pre-amplifier and fed into a four-channel digitizing oscilloscope, with a sampling rate of 200 MHz.

All measurements were done on suspensions consisting of iron ore particles and water. The diameter of the particles varied from 0 μm to 100 μm, which is much smaller than the wavelength of the sound. This means that the long wavelength limit is valid and that the scattering mechanisms derived from that are dominating (see for example [3]). Measurements were performed for mass fractions between 0 and 15 percent.

[1]Panametrics XMS310 miniature immersion transducers

3 Theory

3.1 Principle

Assume that the shape of the energy lobe from the transmitting transducer depends on the particle concentration. One way to measure the change in shape of the lobe is to use several receiving transducers. Figure 2 shows this for the case with one transmitter and two receivers, as used in our experiments.

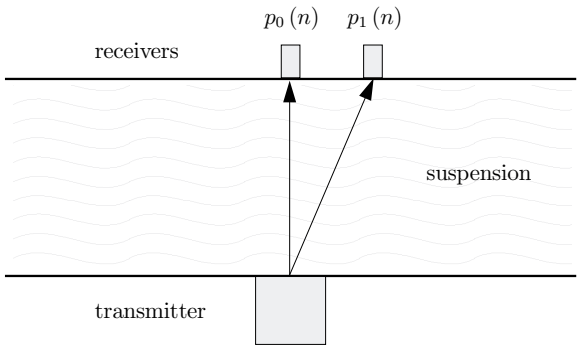

Figure 2: Experimental setup with one transmitting transducer and two receivers.

Since both receivers simultaneously measure the same transmitted pulse, the received energy can be expected to be heavily dependent. It is therefore possible to compare the received pulses pair-wise, and then averaging over several measurements. A simple way to estimate the shape of the lobe is to calculate the received energy at each receiver. To determine how the transmitted energy spreads, we divide the received energy at receiver 1 with the received energy at receiver 0, and then take the average of these ratios for M subsequent measurements. We define the average energy ratio as

$$E = \frac{1}{M} \sum_{m=1}^{M} \frac{E_{m,1}}{E_{m,0}} = \frac{1}{M} \sum_{m=1}^{M} \frac{\sum_{n=1}^{N} p_{m,1}^2(n)}{\sum_{n=1}^{N} p_{m,0}^2(n)}, \tag{1}$$

where $E_{m,0}$ is the energy of m:th received pulse at receiver 0 and $E_{m,1}$ is the energy of m:th received pulse at receiver 1. Measurements indicate that for the concentration interval of interest, the ratio of energies depends on the particle mass fraction as

$$E(c) \approx \alpha_0 + \alpha_1 c, \tag{2}$$

where c is the mass fraction of particles and α_0 and α_1 are constants.

3.2 Calibration

For a specific system, with a given type of particles, the proposed method can be calibrated by making a least squares estimate of the parameters α_0 and α_1 in equation (2).

To fit a straight line we need to measure and calculate the energy ratio for at least two different concentrations. We suggest calibrating at the lowest and highest concentration of interest, at least. The need of calibration is a disadvantage, but as will be shown in the next section, the concentration interval for which the straight line approximation is valid is quite wide.

3.3 On-line measurements

Since the relationship between particle mass fraction and the energy ratio in equation (1) can be approximated by a straight line, measuring the mass fraction is done by calculating the energy ratio and solving the equation

$$c = \frac{E\left(c\right) - \alpha_0}{\alpha_1}. \tag{3}$$

4 Experimental Results

In this section we describe the measurements made, and analyze the uncertainties involved in the mass fraction determination.

4.1 Measurements

As described in section 2, measurements were made with mass fractions of iron ore particles from 0 to 15 percent. For each particle concentration the average energy ratio for 100 received pulses was determined. The result is shown in figure 3.

In figure 3 we see that the approximation of a straight line is valid from about 3 percent and up. The straight line was estimated for this interval, and has equation

$$E(c) = 0.020 + 0.242c \tag{4}$$

We also note that the energy ratio E increases with increased particle mass fraction. This indicates that the lobe from the transmitter is widened when concentration of scattering particles is increased.

For mass fractions of lower than three percent, the energy ratio in equation (1) did not show the same linear dependency on the mass fraction. Also, the variation in energy for the 100 measured pulses was larger for these concentrations (see figure 4). One explanation to this could be that the suspension is less homogeneous for lower mass fractions, resulting in larger variations in amplitude of the received pulses. Also, it might be the case that the dominating scattering mechanism changes at a certain concentration.

4.2 Uncertainty analysis

In this section we analyze the statistical properties of the proposed method, in order to estimate the uncertainty of the concentration measurements. Assume that the energy ratios of the received ultrasonic pulses can be regarded as random variables with the same, but unknown distribution. The central limit theorem [4] states that the average

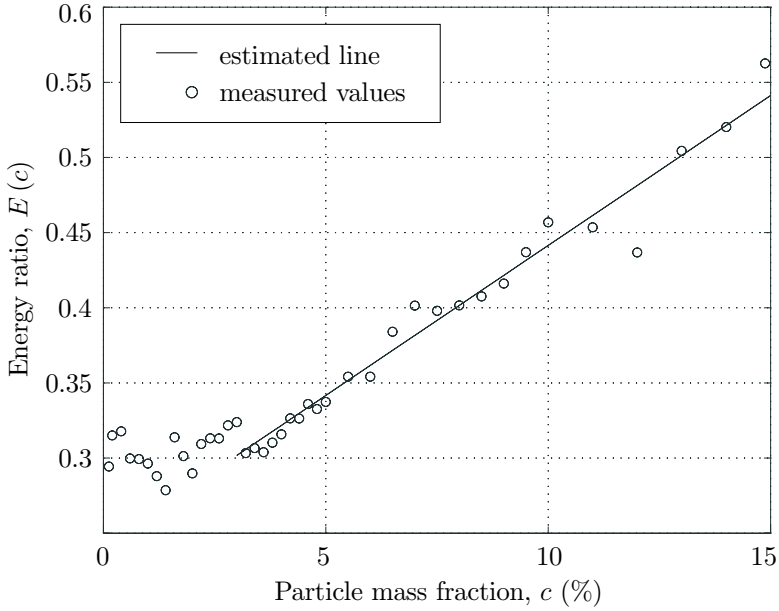

Figure 3: Average energy ratio as a function of particle mass fraction in a suspension of iron ore and water. The estimated line was obtained using a least squares fit to the measured values.

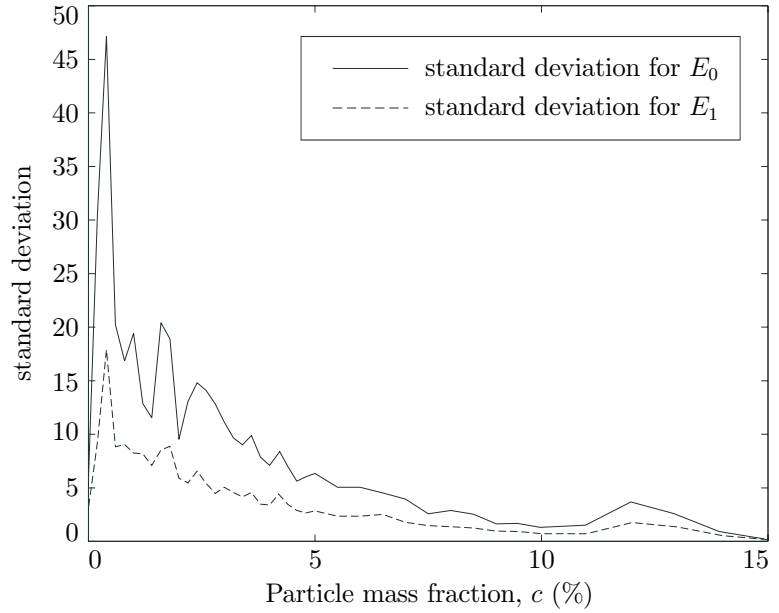

Figure 4: Standard deviation of the energies, measured at receiver 0, 1 respectively.

of several random variables from the same parent distribution will be more and more normally distributed as the number of measurements increase. Thus, the average energy ratio E in equation (1) can be assumed to be normally distributed. A 95% confidence

interval can be determined for each concentration using equation (5) as

$$E_{95}(c) = E(c) \pm t_{95}(M-1)\widehat{\sigma}_{\text{ratio}}, \tag{5}$$

where $t_{95}(M-1)$ is the value of the t-distribution at 95% confidence level and $M-1$ degrees of freedom. In this case, where $M = 100$, the t_{95}-value is approximately 1.98. The confidence intervals are plotted in figure 5.

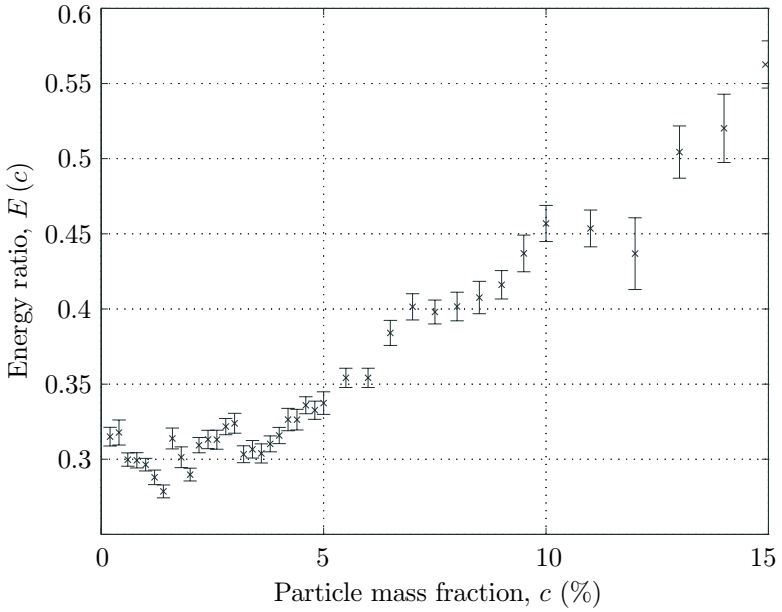

Figure 5: Energy ratio as a function of particle mass fraction, with 95% confidence interval.

In figure 5 we see that the confidence interval becomes wider with larger mass fractions. This phenomenon can be explained by the fact that the signal-to-noise ration (SNR) decreases as concentration increases. This is because the overall attenuation increases, causing the signal level to decrease.

The uncertainty analysis indicates that it should be possible to measure the mass fractions in the interval 3 to 15 percent, with an accuracy of ± 1 percent of the mass fraction. If the confidence interval becomes to wide, this is easily compensated for by increasing the number of measurements for those concentrations.

5 Conclusions

In this paper propose a simple and fast method that can be used to measure particle concentration in multiphase flows. This is illustrated with experiments with iron ore particles and water. The uncertainty analysis shows that it is possible to determine mass fractions with an error of less than 1% of the mass fraction. We have also showed that if we use two receivers, the average energy ratio in equation (1) depends linearly on the mass fraction in the range 3% to 15%. This makes it easy to calibrate, and once the

linear dependency has been determined, online measurements can be done, for a quite wide concentration interval.

For concentrations below three percent, the variation in pulse energies is very large and our method will not give accurate results.

We also see show the advantage of using two receivers is that we are able to block the measurements in pairs, which results in a significantly lower variation in the measured ratio than if the attenuation had been measured in only one point. This result should be possible to extend to more than two receivers, and will be one of the objectives of our future research.

If we combine the proposed method with some conventional transit-time bulk flow meter, for example the sing-around flow meter [6], this can lead to a method for measuring particle mass flows in multiphase flows.

6 Acknowledgements

The authors would like to express their gratitude towards Prof. Kerstin Vännman, Mr. Roger Öström and Mr. Svante Johansson for their valuable input on the uncertainty analysis. We would also like to thank Prof. Jerker Delsing for proof reading and for his valuable comments.

Generous grants from the *Swedish Research Council for Engineering Sciences* is also gratefully acknowledged.

References

[1] Chaoki, J., Larachi, L., and Dudoković, M. P., *Non-Invasive Monitoring of Multiphase Flows.* Elsevier, 1997.

[2] Whitaker, T. S., "A Review of Multiphase Flowmeters and Future Development Potential," in *Flow Measurement: Proceedings of the 6th Int. Conf. on Flow Measurement FLOMEKO'93.* (Seoul, Korea), pp. 628-634, Oct. 1993.

[3] Povey, M. J. W., *Ultrasonic Techniques for Fluid Characterization.* Academic Press, 1997.

[4] Box, G. E. P., Hunter, W. G., and Hunter, J. S., *Statistics for Experimenters.* John Wiley and Sons, 1978.

[5] Coleman, H. W. and Steele, W. G., *Experimentation and Uncertainty Analysis for Engineers.* John Wiley and Sons, 1989.

[6] Lynnworth, L. C., *Ultrasonic Measurements for Process Control.* Academic Press, 1989.

Paper C

A Fast Algorithm for Generating Optimal Designs for Regression Problems

Authors:
Johan Carlson, Anders Grennberg, and Rolf Carlson

To be submitted

A Fast Algorithm for Generating Optimal Designs for Regression Problems

Johan Carlson, Anders Grennberg, and Rolf Carlson

Abstract

In a screening experiment very little is known about the underlying model, and the objective is to fit a simple model that can be used to find smaller test systems. In this paper we propose an algorithm for constructing optimal experimental designs for this kind of experiments. The algorithm is used iteratively to select one experiment at a time until the estimated model parameters are good enough. The optimality criterion is to minimize the mean squared error of the estimated model parameters. The performance of the algorithm is illustrated with a practical example, and we show that the algorithm works when other criteria, such as D-optimality, does not.

1 Introduction

When faced with a new experimental situation, often nothing or little is known about the factors affecting the outcome of the experiments. In a screening experiment the objective is to cover as much of the experimental variation as possible in a fairly small number of experiments. This will then give information about smaller test systems for further exploration.

1.1 Experimental Strategy

We suggest the following strategy for performing a first screening of a new experimental situation.

1. Analyze the problem and determine which factors are likely to affect the outcome. Determine which response(s) should be measured.

2. Determine the candidate design matrix as a full factorial design given by all possible combinations of the discrete settings of the factors. The variables should be centered around a working point.

3. Assign a tentative Taylor expansion model for the screening.

4. Compute the candidate model matrix $\mathbf{X}$ by appending columns corresponding to terms in the model (constant, cross-product and square terms).

5. Select experiments from the candidate model matrix that covers as much of the total experimental variation as possible.

6. If desired, select additional experiments to improve the model fit.

7. Run the experiments and fit the model. Assess the significance of the variables.

8. Confirm conclusions by experiments.

In this paper we derive an algorithm that can be used for the selection of candidate experiments, as indicated in 5 and 6 above.

1.2 Previous Work

A large amount of work has been done in the area of regression analysis and experimental design. A set of optimality criteria discussed in [1] and the application to regression analysis was considered in [2]. Although there are several different criteria to choose among, many methods concerning optimal designs seem to focus on the D-optimality criterion. The goal with such a design is to select the experimental model matrix $\mathbf{X}$ so that the determinant of $\mathbf{X}^T\mathbf{X}$ is maximized (see for example [3]). Often the experiments must be selected as a subset of a larger number of candidate experiments, and can not be designed arbitrarily. There are several algorithms available for the construction of D-optimal designs, such as Fedorov's algorithm of exchange [3] and Mitchell's DETMAX [4].

Other examples of exchange algorithms are the coordinate exchange algorithm [5] and columnwise algorithms [6]. These algorithms perform well and has been shown to be faster than for example Fedorov's algorithm.

In some practical cases, as we will show later, the model matrix or the candidate matrix does not have full column rank. In these cases, the D-optimality criterion is not relevant, since the determinant of $\mathbf{X}^T\mathbf{X}$ is always zero. In order for any of the mentioned methods to work, the model has to be changed by removing columns. In a new experimental situation, where little is known about the underlying model, this is very difficult. A paper previously presented by the authors [7] used a modified model and D-optimality to generate a design for the experiment presented later in this paper.

2 Problem Description

Assume that we can describe the functional relationship between physical variables and the experimental output as

$$y = f(x_1, x_2, ..., x_N) + \varepsilon. \tag{1}$$

The function f can also be represented by its Taylor expansion as

$$f = \beta_0 + \sum_{i=1}^{N} \beta_i x_i + \sum_{i=1}^{N}\sum_{j=1}^{N} \beta_{ij} x_i x_j + \text{ higher order terms.} \tag{2}$$

Often it is sufficient to approximate the function using the linear, cross product, and square terms in the Taylor expansion. This can be expressed in vector notation as

$$f = \mathbf{x}^T\mathbf{b} = \begin{bmatrix} 1 & x_1, & x_2, & \ldots, & x_N^2 \end{bmatrix} \begin{bmatrix} \beta_0 \\ \beta_1 \\ \vdots \\ \beta_N^2 \end{bmatrix}. \tag{3}$$

If M experiments are performed, this can be written as

$$\begin{bmatrix} f_1 \\ f_2 \\ \vdots \\ f_M \end{bmatrix} = \begin{bmatrix} 1 & x_{11} & x_{12} & \cdots & x_{1k}^2 \\ 1 & x_{21} & x_{22} & \cdots & x_{2k}^2 \\ 1 & \vdots & \ddots & & \vdots \\ 1 & x_{M1} & x_{M2} & \cdots & x_{Mk}^2 \end{bmatrix} \begin{bmatrix} \beta_0 \\ \beta_1 \\ \vdots \\ \beta_{kk} \end{bmatrix}. \tag{4}$$

Assume that the observed experimental results is

$$\mathbf{y} = \mathbf{f} + \boldsymbol{\varepsilon}. \tag{5}$$

A least squares estimate of the model parameter vector $\mathbf{b}$ is then given by

$$\widehat{\mathbf{b}} = \mathbf{X}^\dagger\mathbf{y}, \tag{6}$$

where $\mathbf{X}^\dagger$ denotes the Moore-Penrose pseudo inverse (see for example [8]). In the special case when $\mathbf{X}$ has full column rank, equation (6) is equivalent to

$$\widehat{\mathbf{b}} = \left(\mathbf{X}^T\mathbf{X}\right)^{-1}\mathbf{X}^T\mathbf{y} \tag{7}$$

The problem of experimental design is to select the matrix $\mathbf{X}$ so that we obtain reliable estimates of the model parameters $\mathbf{b}$. In the next section we first define an optimality criterion for the construction of $\mathbf{X}$, and then derive an algorithm that fulfills it.

Another constraint on $\mathbf{X}$ is that the rows must be chosen among the rows of a larger candidate model matrix $\mathbf{C}$. The candidate model matrix is constructed as the full factorial design matrix appended with a column of ones and columns for cross-terms and squared variable terms.

3 The Algorithm

In this section we first derive and motivate a new optimality criterion for the design of a screening experiments. We then propose an algorithm for constructing such designs. The algorithm constructs a model matrix by selecting one row at a time from the candidate model matrix and appending it to the design. For each new row that is added to the design the rank is increased by one, until the rank of the candidate model matrix is reached.

3.1 Optimality Criterion

If we want to use the model in equation (3) to predict the outcome of future experiments, it is important that the estimate of the model parameters $\mathbf{b}$ are accurate. Therefore, we define the optimal model matrix $\mathbf{X}$ as the matrix minimizing

$$J = E\{\|\mathbf{b} - \widehat{\mathbf{b}}\|^2\}. \tag{8}$$

Expanding (8) gives

$$J = E\left\{\|\mathbf{b} - \widehat{\mathbf{b}}\|^2\right\} = E\left\{\left(\widehat{\mathbf{b}}-\mathbf{b}\right)^T\left(\widehat{\mathbf{b}}-\mathbf{b}\right)\right\}. \tag{9}$$

Inserting (6) into (9) yields

$$J = E\left\{\left(\mathbf{X}^\dagger\mathbf{y} - \mathbf{b}\right)^T\left(\mathbf{X}^\dagger\mathbf{y} - \mathbf{b}\right)\right\}. \tag{10}$$

Under the assumption that the experimental error $\boldsymbol{\varepsilon}$ is independent of $\mathbf{X}$ and $E\{\boldsymbol{\varepsilon}\} = 0$, we obtain

$$\begin{aligned} J &= E\left\{\left(\mathbf{X}^\dagger\mathbf{f} + \mathbf{X}^\dagger\boldsymbol{\varepsilon} - \mathbf{b}\right)^T\left(\mathbf{X}^\dagger\mathbf{f} + \mathbf{X}^\dagger\boldsymbol{\varepsilon} - \mathbf{b}\right)\right\} \\ &= E\left\{\left(\mathbf{X}^\dagger\mathbf{X}\mathbf{b} + \mathbf{X}^\dagger\boldsymbol{\varepsilon} - \mathbf{b}\right)^T\left(\mathbf{X}^\dagger\mathbf{X}\mathbf{b} + \mathbf{X}^\dagger\boldsymbol{\varepsilon} - \mathbf{b}\right)\right\} \\ &= E\left\{\left(\mathbf{b}^T\mathbf{X}^T\mathbf{X}^{\dagger T} + \boldsymbol{\varepsilon}^T\mathbf{X}^{\dagger T} - \mathbf{b}^T\right)\left(\mathbf{X}^\dagger\mathbf{X}\mathbf{b} + \mathbf{X}^\dagger\boldsymbol{\varepsilon} - \mathbf{b}\right)\right\} \\ &= E\left\{\mathbf{b}^T\mathbf{X}^T\mathbf{X}^{\dagger T}\mathbf{X}^\dagger\mathbf{X}\mathbf{b} - \mathbf{b}^T\mathbf{X}^T\mathbf{X}^{\dagger T}\mathbf{b} + \boldsymbol{\varepsilon}^T\mathbf{X}^{\dagger T}\mathbf{X}^\dagger\boldsymbol{\varepsilon} - \mathbf{b}^T\mathbf{X}^\dagger\mathbf{X}\mathbf{b} + \mathbf{b}^T\mathbf{b}\right\}. \end{aligned} \tag{11}$$

Since $\mathbf{X}^\dagger\mathbf{X}$ is a projection matrix $\mathbf{P}_\mathbf{X}$ onto the row space of $\mathbf{X}$, (see for example chapter 5 in [8]), equation (11) simplifies to

$$\begin{aligned} J &= E\left\{\mathbf{b}^T\mathbf{P}_\mathbf{X}\mathbf{b} - \mathbf{b}^T\mathbf{P}_\mathbf{X}\mathbf{b} + \boldsymbol{\varepsilon}^T\mathbf{X}^{\dagger T}\mathbf{X}^\dagger\boldsymbol{\varepsilon} - \mathbf{b}^T\mathbf{P}_\mathbf{X}\mathbf{b} + \mathbf{b}^T\mathbf{b}\right\} \\ &= E\left\{\boldsymbol{\varepsilon}^T\mathbf{X}^{\dagger T}\mathbf{X}^\dagger\boldsymbol{\varepsilon} - \mathbf{b}^T\mathbf{P}_\mathbf{X}\mathbf{b} + \mathbf{b}^T\mathbf{b}\right\} \\ &= E\left\{\boldsymbol{\varepsilon}^T\mathbf{X}^{\dagger T}\mathbf{X}^\dagger\boldsymbol{\varepsilon} + \mathbf{b}^T\left(\mathbf{I} - \mathbf{P}_\mathbf{X}\right)\mathbf{b}\right\} \\ &= E\left\{\boldsymbol{\varepsilon}^T\mathbf{X}^{\dagger T}\mathbf{X}^\dagger\boldsymbol{\varepsilon} + \mathbf{b}^T\mathbf{P}_\mathbf{X}^\perp\mathbf{b}\right\} \\ &= E\left\{\boldsymbol{\varepsilon}^T\mathbf{X}^{\dagger T}\mathbf{X}^\dagger\boldsymbol{\varepsilon}\right\} + \|\mathbf{P}_\mathbf{X}^\perp\mathbf{b}\|^2, \end{aligned} \tag{12}$$

where $\mathbf{P}_\mathbf{X}^\perp$ is the projection matrix that projects on the orthogonal complement of the row space of $\mathbf{X}$, that is, a projection onto the null space of $\mathbf{X}$. If $\mathbf{X}$ is constructed as we propose in the next section, this term will decrease when the rank of $\mathbf{X}$ increases. Thus, if $\mathbf{X}$ has full column rank, the null space has dimension zero, and the second term in (12) vanishes and the variance of coefficient estimation error reduces to

$$J = E\left\{\boldsymbol{\varepsilon}^T\mathbf{X}^{\dagger T}\mathbf{X}^\dagger\boldsymbol{\varepsilon}\right\}. \tag{13}$$

If $\mathbf{X}$ does not have full column rank, it will lead to a constant error remaining after *maximum* rank has been achieved. This error will not decrease even if the design is appended with more experiments. However, by using the pseudo-inverse to estimate the model parameters, we make sure that the solution lies within the row space of $\mathbf{X}$.

Theorem 1 *If the experimental noise $\boldsymbol{\varepsilon}$ has diagonal covariance matrix, $\theta = E\{\boldsymbol{\varepsilon}\boldsymbol{\varepsilon}^T\}$ of the form $\mathbf{I}\cdot\eta^2$, minimizing (13) is equivalent to minimizing*

$$\sum_{k=1}^{r} \frac{1}{\sigma_k^2}, \tag{14}$$

where σ_k^2 $(k = 1, 2, \ldots r)$ are the eigenvalues of $\mathbf{X}^T\mathbf{X}$ and r is the rank of $\mathbf{X}$. See Appendix A for proof.

The harmonic mean of $\sigma_1^2, \sigma_2^2, \ldots, \sigma_r^2$ is

$$H = \left(\frac{1}{r} \sum_{k=1}^{r} \frac{1}{\sigma_k^2} \right)^{-1}. \tag{15}$$

Thus, the theorem says that the harmonic mean should be maximized.

The criterion of A-optimality (see for example [3]) states that the sum $\sigma_1^2+\sigma_2^2+\ldots+\sigma_r^2$ should be maximized, that is, the arithmetic mean of the singular values should be maximized. A well-known inequality [9] says that the harmonic mean is always less than or equal to the arithmetic mean, with equality if and only if all σ_k are equal. A-optimality does not consider the relationship between different σ_k. For a given value of the arithmetic mean, it is still possible to increase the harmonic mean by appending rows so that the ratio between the largest and the smallest singular values, σ_1/σ_r, decreases.

The goal of the second step of the proposed algorithm is to minimize the difference between all σ_k^2. This will also improve the condition number of the design matrix, which leads to more stable estimates of the model parameters.

3.2 Step I: Creating a Maximum Rank Matrix X

Any $m \times n$ matrix $\mathbf{C}$ can be factored into

$$\mathbf{C} = \mathbf{U}\boldsymbol{\Sigma}\mathbf{V}^T, \tag{16}$$

where the columns of $\mathbf{U}$ are eigenvectors of $\mathbf{C}\mathbf{C}^T$, and the columns of $\mathbf{V}$ are eigenvectors of $\mathbf{C}^T\mathbf{C}$. If the rank of $\mathbf{C}$ is r, the r singular values on the diagonal of $\boldsymbol{\Sigma}$ are the square roots of the nonzero eigenvalues of $\mathbf{C}\mathbf{C}^T$ and $\mathbf{C}^T\mathbf{C}$. Furthermore, if $\mathbf{C}$ has rank r, the first r columns of $\mathbf{V}$ form an orthogonal basis for the row space of $\mathbf{C}$, and the r first columns of $\mathbf{U}$ form an orthogonal basis for the column space of $\mathbf{C}$. Another useful property of the columns in $\mathbf{V}$ is that the first one points out the direction in which we have the largest variation in the row space, the next column points out the second most important direction, *etc.* If we, using as few experiments as possible, wish to span the row space of $\mathbf{C}$, and at the same time cover as much of the total variation as possible, selecting the experiments as the r first columns of $\mathbf{V}$ is optimal. In a real-life situation, however, it is not likely that we can set up experiments that satisfy this. What we can do instead, is to select the row in $\mathbf{C}$ that is the most parallel to the first column in $\mathbf{V}$. That is, choose the row $\mathbf{c}_i^T$ in $\mathbf{C}$ that maximizes the absolute value of the scalar product $\mathbf{c}_i^T\mathbf{v}_1$.

When the first experiment has been selected, we can remove the component in this direction from all rows in $\mathbf{C}$. The resulting matrix will have rank exactly one less than

C. Removing the projection onto row $\mathbf{c}_i^T$ from all other rows $\mathbf{c}_k^T$ is made according to equation (17)

$$\widehat{\mathbf{c}}_k = \mathbf{c}_k - \frac{\left(\mathbf{c}_i^T \mathbf{c}_k\right)}{\mathbf{c}_i^T \mathbf{c}_i} \mathbf{c}_i. \tag{17}$$

Below, we explain how this procedure can then be repeated to select as many rows as the rank r of the candidate matrix. The algorithm can be summarized in the following steps:

1. Let $\mathbf{C}_\mathrm{o}$ be the original candidate matrix, consisting of all possible experiments.

2. Factor $\mathbf{C}_j$ (where $\mathbf{C}_j$ is the candidate matrix after j iterations) in $\mathbf{U}, \mathbf{\Sigma}$, and $\mathbf{V}$ using *singular value decomposition* (SVD).

3. Select the row $\mathbf{c}_i^T$ from $\mathbf{C}_j$ that is most parallel to the first column in $\mathbf{V}$, by finding the row that maximizes $\mathrm{abs}\left(\mathbf{c}_i^T \mathbf{v}_1\right)$. Add the corresponding row of $\mathbf{C}_\mathrm{o}$ to the model matrix $\mathbf{X}$.

4. Construct a new matrix $\mathbf{C}_{j+1}$ where the rows $\widehat{\mathbf{c}}_k^T$ are defined by equation (17).

5. Repeat from step 2 until the desired number of experiments has been selected (less than or equal to the rank of $\mathbf{C}_\mathrm{o}$).

3.3 Step II: Appending More Rows to the Design

The first step of the algorithm, as presented above, yields a design which spans the row space of the candidate model matrix. It is, however, possible to decrease the uncertainty in the model parameters by performing additional experiments. In this section, we show how to do this so that (14) will be minimized.

To include additional rows, we select the row that increases the smallest singular value of $\mathbf{X}$ the most. This is achieved by selecting the row that has the largest component in the direction of $\mathbf{v}_r^T$, i.e., the singular vector corresponding to the smallest singular value. The reason for this is that no singular value can decrease if a matrix is appended with an additional row [10], and the sum in equation (14) will be smallest if all σ_k^2 are equal. The implementation of this is very similar to the implementation of the first step of the algorithm.

4 Application Example

In this section we give a practical example to illustrate the usefulness of the proposed algorithm.

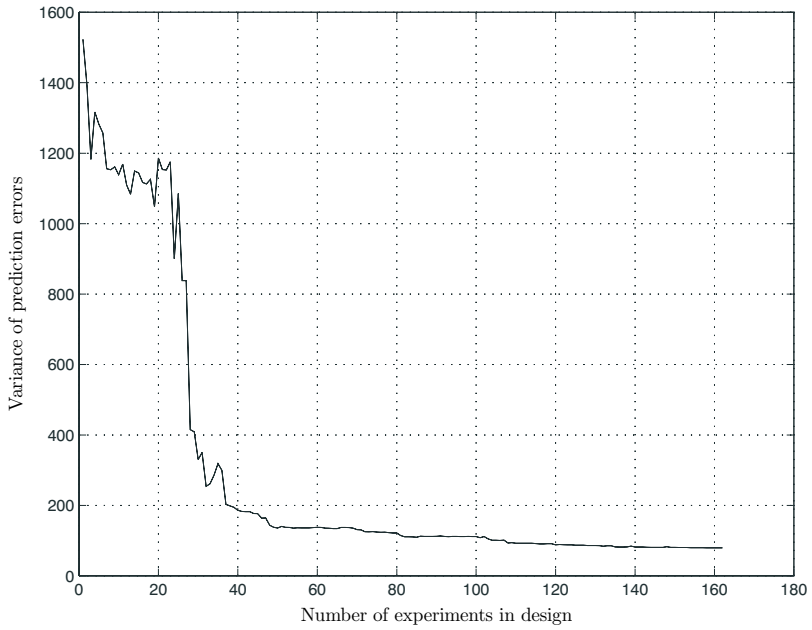

Figure 1: Performance of the proposed algorithm. The variance of the prediction errors plotted as a function of the number of experiments used to estimate the model parameters.

4.1 Problem Description

The acid catalyzed rearrangement of phenyl hydrazones from ketones is known as the Fischer indole synthesis. Phenyl hydrazones derived from dissymmetric ketones can give rise to two regioisomeric indoles. An extensive study to clarify the roles played by the properties of the catalysts and solvents for determining the regioselectivity of the reaction has been published by Prochazka and Carlson [11]. The problem to solve was to determine whether or not there exists a combination of catalysts and solvents which can give a regioselective reaction.

To illustrate the strategy suggested in this paper we will use the data from [12]. The total number of possible combinations of ketones, catalysts, and solvents was 600 experiments. Of these, 296 were tested experimentally, and out of these, 162 experiments afforded the Fischer indole reaction. With a second order Taylor model of the form (2), this resulted in a candidate model matrix with 44 columns. The rank was found to be 35.

4.2 Results

A Taylor model of the form (2) was used to predict the experimental yield y. The model parameters $\mathbf{b}$ was estimated using observed experimental yield from a number of experiments selected with the proposed algorithm. In figure 1 we have plotted the variance of the prediction errors as a function of the number of experiments in the design. This is a measure of the model fit, as a function of the number of experiments. We see in the figure that around 50 experiments was enough to get good estimates of the

model parameters. The candidate model matrix had rank 35 and consisted of the 162 experiments described above.

5 Conclusions

In the previous section we used the algorithm to construct a prioritized list of experiments. We also see in figure 1 using a design based on only a few more experiments than the numerical rank of the candidate model matrix, is enough to obtain good estimates of the model parameters. In a new experimental situation it is, of course, not possible to decide how many experiments should be enough. We suggest that, in a first run, the experimenter should perform at least as many experiments as the numerical rank of the candidate model matrix, and then use the prioritized list given by the algorithm and continue until the change in the model parameters is small enough.

A drawback with many of the exchange based algorithms is that they require an initial design. Often the problem of constructing the initial design is not handled, even though the result depends very much on it. This is the case in, for example, Fedorov's algorithm of exchange [3]. These algorithms are often iterative and the rate of convergence often depends on the initial design. This is not the case for the proposed algorithm, since each experiment that should be added to the design is completely determined by a fixed number of calculations. Another advantage that makes the proposed algorithm especially useful in a new experimental situation is that it can be used in a sequential manner, that is, to include one experiment to the design at a time without having to regenerate the entire design.

D-optimality is not relevant when the candidate model matrix does not have full column rank, since the determinant of $\mathbf{X}^T\mathbf{X}$ is always zero. In order to be able to use algorithms based on D-optimality, the experimenter has to make sure that the candidate model matrix $\mathbf{X}$ has full rank, by removing columns. In a screening experiment, where very little is known about the underlying model, this is difficult. In a previous paper [7], we used a Taylor model without the squared terms together with D-optimality and Fedorov's algorithm of exchange [3]. With the method presented in this paper, the model fit is better and the algorithm is much faster and much more stable.

A Proof of theorem 1

In this appendix we prove that minimizing

$$J = E\left\{\boldsymbol{\varepsilon}^T\mathbf{X}^{\dagger T}\mathbf{X}^{\dagger}\boldsymbol{\varepsilon}\right\}, \tag{18}$$

is equivalent to minimizing

$$\sum_{k=1}^{r}\frac{1}{\sigma_k^2}. \tag{19}$$

Since the expression inside the brackets in (18) is a scalar, this is equal to minimizing

$$J = E\left\{\mathrm{tr}\left(\boldsymbol{\varepsilon}^T\mathbf{X}^{\dagger T}\mathbf{X}^{\dagger}\boldsymbol{\varepsilon}\right)\right\}. \tag{20}$$

Noting that $\mathrm{tr}(\mathbf{AB}) = \mathrm{tr}(\mathbf{BA})$, equation (20) can be rewritten as

$$J = \mathrm{tr}\left(\mathbf{X}^{\dagger} E\{\boldsymbol{\varepsilon}\boldsymbol{\varepsilon}^T\}\mathbf{X}^{\dagger T}\right). \tag{21}$$

We define the covariance matrix θ as

$$\theta = E\left\{\boldsymbol{\varepsilon}\boldsymbol{\varepsilon}^T\right\}, \tag{22}$$

which leads to

$$J = \mathrm{tr}\left(\mathbf{X}^{\dagger}\theta\mathbf{X}^{\dagger T}\right). \tag{23}$$

When $\mathbf{X}$ is factored using the SVD, as

$$\mathbf{X} = \mathbf{U}\boldsymbol{\Sigma}\mathbf{V}^T, \tag{24}$$

the pseudo-inverse $\mathbf{X}^{\dagger}$ is given by,

$$\mathbf{X}^{\dagger} = \mathbf{V}\boldsymbol{\Sigma}^{\dagger}\mathbf{U}^T, \tag{25}$$

where the diagonal of $\boldsymbol{\Sigma}^{\dagger}$ $(n \times m)$ contains the reciprocals $1/\sigma_1, \ldots, 1/\sigma_r$ of the non-zero diagonal of $\boldsymbol{\Sigma}$ $(m \times n)$ $\sigma_1, \ldots \sigma_r$. All other elements of $\boldsymbol{\Sigma}^{\dagger}$ are zero. Inserting this into (23), we obtain

$$J = \mathrm{tr}\left(\mathbf{V}\boldsymbol{\Sigma}^{\dagger}\mathbf{U}^T\theta\mathbf{U}\boldsymbol{\Sigma}^{\dagger T}\mathbf{V}^T\right). \tag{26}$$

Considering the special case when $\theta = \mathbf{I}\cdot\eta^2$, equation (23) reduces to

$$J = E\left\{\mathrm{tr}\left(\mathbf{V}\boldsymbol{\Sigma}^{\dagger}\boldsymbol{\Sigma}^{\dagger T}\mathbf{V}^T\right)\right\}\cdot\eta^2. \tag{27}$$

Since the trace operator is invariant to a change of basis, this is equivalent to

$$J = E\left\{\mathrm{tr}\left(\boldsymbol{\Sigma}^{\dagger}\boldsymbol{\Sigma}^{\dagger T}\right)\right\}\cdot\eta^2 = \left(\sum_{k=1}^{r}\frac{1}{\sigma_k^2}\right)\eta^2, \tag{28}$$

which leads to the criterion that the trace of $\boldsymbol{\Sigma}^{\dagger}\boldsymbol{\Sigma}^{\dagger T}$should be minimized, that is

$$\min_{\mathbf{X}}\sum_{k=1}^{r}\frac{1}{\sigma_k^2}, \tag{29}$$

where σ_k^2, $k = 1, 2, \ldots r$ are the eigenvalues of $\mathbf{X}^T\mathbf{X}$ and r is the rank of $\mathbf{X}$.

Q.E.D.

References

[1] J. Kiefer, "On the Nonrandomized Optimality and the Randomized Nonoptimality of Symmetrical Designs," *Ann. Math. Stat.*, 29, 675-699, 1958.

[2] J. Kiefer and J. Wolfowitz, "Optimum Designs in Regression Problems," *Ann. Math. Stat.*, 30, 271-294, 1959.

[3] V. Fedorov, *Theory of Optimal Experiments*, Academic Press, 1972.

[4] T. K. Mitchell, "An algorithm for the Construction of D-Optimal Designs," *Technometrics*, 16, 203-210, 1974.

[5] R. K. Meyer and C. J. Nachtsheim, "The Coordinate-Exchange Algorithm for Constructing Exact Optimal Experimental Designs," *Technometrics*, 37, 60-69, 1995.

[6] W. W. Li and C. F. J. Wu, "Columnwise-Pairwise Algorithms With Applications to the Construction of Supersaturated Designs," *Technometrics*, 39, 171-179, 1997.

[7] R. Carlson and J. Carlson, "Strategy for Screening Discrete Variations in Organic Synthesis," in *Proc. Chimiométrie 97,* (Lyon, France), C11-1 - C11-12, Nov. 1997.

[8] G. H. Golub and C. F. Van Loan, *Matrix Computations*, Johns Hopkins, 1996.

[9] G. H. Hardy, J. E. Littlewood, and G. Pólya, *Inequalities*, Cambridge, 1964.

[10] Å. Björck, *Numerical Methods for Least Squares Problems*, SIAM, 1996.

[11] M. P. Prochazka and R. Carlson, "On the role of Lewis acid catalysts and solvents in the Fischer indole synthesis," *Acta Chem. Scand.*, 43, 651-659, 1989.

[12] R. Carlson, *Design and Optimization in Organic Synthesis*, Elsevier, 1992.